Microfluid Nanofluid (2015) 18:233–243
DOI 10.1007/s10404-014-1423-x

RESEARCH PAPER

A mathematical model for nanoparticle melting with density change

F. Font · T. G. Myers · S. L. Mitchell

Received: 4 February 2014 / Accepted: 10 May 2014 / Published online: 24 May 2014

Abstract The melting process of a spherical nanoparticle is analysed using a mathematical model derived from continuum theory. The standard model for macro-scale melting is modified to include melting point depression using the Gibbs–Thomson equation. The key difference between the current and previous work in the melting of nanoparticles is that the difference in densities between the solid and liquid phases is accounted for. This modifies the energy balance at the phase change interface to include a kinetic energy term, which then changes the form of the equation, and it also requires an advection term in the heat equation for the liquid phase. Approximate analytical and numerical solutions are presented for the melting of particles in the range 10–100 nm. It is shown that when the density difference is included in the model, melting is significantly slower than when density is assumed constant throughout the process. This is attributed to the flowing liquid providing a sink term, namely kinetic energy, in the energy balance. The difference in results is greatest for small particles; however, it is concluded that the varying density model will never reduce to the constant density model resulting in a difference of around 15 % even at the macro-scale.

Keywords Phase change · Nanoparticle · Expansion · Melting

F. Font · T. G. Myers (✉)
Centre de Recerca Matemàtica, Campus de Bellaterra, Edifici C, 08193 Bellaterra, Barcelona, Spain
e-mail: tmyers@crm.cat

F. Font
e-mail: ffont@crm.cat

F. Font · T. G. Myers
Departament de Matemàtica Aplicada I, Universitat Politècnica de Catalunya, Barcelona, Spain

S. L. Mitchell
MACSI, Department of Mathematics and Statistics, University of Limerick, Limerick, Ireland
e-mail: sarah.mitchell@ul.ie

1 Introduction

There exists a large body of work concerning the mathematical modelling of phase change, which is often termed a Stefan problem. The original Stefan problem concerned the formation of sea ice. Since then, the model has been applied to many different forms of phase change and geometries as well as topics in porous media flow and finance (Ockendon et al. 1999). An analogous problem occurs in the growth of material from a saturated liquid, where concentration rather than temperature gradients drives the growth (Davis 2001). In the context of phase change, the vast majority of studies incorporate a number of restrictive assumptions, which are often made for mathematical convenience and limit the applicability of the results to highly idealised situations. Alexiades and Solomon (1993, Chap. 1) provide a list of standard assumptions including constant latent heat, constant phase change temperature, a sharp phase change interface, constant thermal properties in each phase and a constant density, which is equal in both phases. They state that this final assumption is perhaps the most unreasonable; indeed, anyone with experience of burst water pipes will be aware of the true importance of density change. Consequently, in this paper, we will focus on the effect of density change. Our work is motivated by the melting of spherical nanoparticles, and however, the model could be applied to more general situations of practical interest, such as pipe

bursting, cryopreservation, phase change microvalves and metal casting, see Alexiades and Solomon (1993), Myers and Low (2011), Myers and Low (2013), Font et al. (2013) and Natale et al. (2010).

In Alexiades and Solomon (1993), freezing and melting with the incorporation of a density change are discussed. They state that most physical properties vary to some extent with temperature, but that at the phase change temperature there is often a sudden change. Although the value of the density may not change as much as other variables, its variation may lead to the most pronounced effects. They subsequently analyse phase change in Cartesian co-ordinates to show that the density jump introduces a nonstandard term, proportional to the cube of the phase change velocity, into the Stefan condition. They discuss how neglecting this term can lead to over- or underestimation of the front velocity depending on the physical situation. However, they later neglect this term to permit exact similarity solutions. Natale et al. (2010) take a similar approach, again to find similarity solutions. Charach and Rubinstein (1992) neglect the cubic term altogether and seek small time and similarity solutions for the freezing of a liquid layer and phase change in a porous half-space. In the following work, we will demonstrate the importance of the cubic term, particularly near the beginning and end of the process.

At the nano-scale, an important effect is that of melting point depression, which can lead to rapid melting as the particle size tends to zero. This may explain the sudden disappearance of particles discussed in Kofman et al. (1999). The variation of the melt temperature with size is often represented by the Gibbs–Thomson equation, although there exist a number of other forms with the common feature that the temperature change is proportional to curvature Buffat and Borel (1976), Kofman et al. (1999), Lai et al. (1996) and Nanda (2009). In the following work, we will employ the classical Gibbs–Thomson relation

$$T_m = T_m^*\left(1 - \frac{2\sigma_{sl}\kappa}{\rho_s L_f}\right) \tag{1}$$

where T_m^* is the bulk melting temperature, σ_{sl} the surface energy between the solid and the liquid, L_f the latent heat and ρ_s the density. The curvature of a sphere is $\kappa = 1/R$, where R is the particle radius. Note, if we take parameter values for gold, as given in Table 1, we find $T_m > 0$ when $R > 0.44$ nm. Assuming our results only hold for $R > 2$ nm, we do not expect mathematical problems to arise due to using the above form of the Gibbs–Thomson relation.

In McCue et al. (2009), small time and large Stefan number solutions are sought for a two-phase problem describing the melting of spherical nanoparticles subject to (1). Font and Myers (2013) focus on the situation where the specific heats vary through the phase change. To account for this, they apply a more general form of the Gibbs–Thomson relation. Their results show that melting point depression is extremely important in predicting the melt time of nanoparticles. They also investigate the effect of using the generalised Gibbs–Thomson relation as opposed to the above classical version. Wu et al. (2009) had previously concluded that melting point depression could explain the rapid melting of nanoparticles. To simplify the mathematics, their work used an approximation where the variation of specific heat was neglected in the generalised Gibbs–Thomson relation [meaning (1) was valid] but retained in the remaining governing equations. In Font and Myers (2013), it was shown that, when compared to using the generalised Gibbs–Thomson relation, this approach leads to differences on the order of 10 % in melt times for 10 nm particles, whilst for 100 nm particles the difference is around 1 %. In the following study, we will see that allowing the density to vary can more than double the melt time of a 10 nm particle. Thus, in order to keep the analysis simple and focus on the density variation, we will assume the specific heats to be equal for both phases and model the melting point depression with (1).

The mathematical model to be developed in the following section will be based on continuum theory. Since our focus is on nanoscale phase change, it is worth considering the validity of this theory. This issue is discussed in detail in Font and Myers (2013). To summarise, they state that comparison of molecular dynamics simulations, experiment and continuum theory has led to the conclusion that for fluid flow, continuum theory may be accurate down to around 3 nm, for heat transfer and phase change, 2 nm appears to be the lower limit, see Guisbiers et al. (2008) and Travis et al. (1997). Consequently, we only expect our model to be valid for particles >2 nm. Note, the Gibbs–Thomson relation (1) requires $R > 2\sigma_{sl}/(\rho_s L_f)(\approx 0.4\,\text{nm}$

Table 1 Approximate thermodynamical parameter values for gold

Substance	T_m^* (K)	L_f (J/Kg)	c_l, c_s (J/Kg K)	ρ_l, ρ_s (kg/m^3)	k_l, k_s (W/m K)	σ_{sl} (N/m)
Gold	1337	6.37×10^4	163/129	$1.73 \times 10^4/1.93 \times 10^4$	106/317	0.27

The value of σ_{sl} is taken from Buffat and Borel (1976)

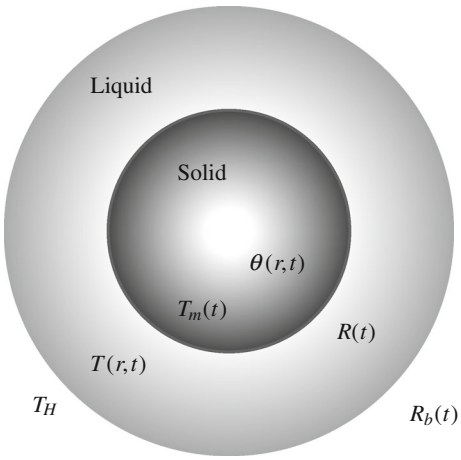

Fig. 1 Sketch of the model, showing a solid sphere of radius $R(t)$ surrounded by a liquid layer with radius $R_b(t)$

for gold). So we may assume Eq. (1) to be accurate for physically realistic values of the continuum model.

In Sect. 2 of this paper, we present a mathematical model that describes the melting of spherical nanoparticles including melting point depression and density change between phases. In Sect. 3, we seek approximate solutions by means of a perturbation method. Then, we pinpoint the small time behaviour of the system and use it later on to initialise the numerical scheme described in Sect. 4. Results are presented in Sect. 5, comparing the numerical and approximate solutions. Finally, in Sect. 6, we present the main conclusions of this study.

2 Mathematical model

We consider a solid sphere with radius R_0, initially at the melting temperature $T_m(R_0)$, which is given by the Gibbs–Thomson Eq. (1). The surface of the sphere is suddenly raised to temperature $T_H > T_m(R_0)$ which starts the melting process: a liquid phase grows inwards from the surface of the particle until the solid disappears. We denote the moving solid–liquid interface by $R(t)$. Due to the density change, the outer surface also moves, and it is designated as $R_b(t)$, where $R_b(0) = R_0$. A sketch of the model is presented in Fig. 1.

To describe the melting process of the nanoparticle requires solving heat equations in the solid and liquid phases over the moving domains $0<r<R(t)$ and $R(t)<r<R_b(t)$, respectively. The heat equation in the liquid is given by

$$\rho_l c_l\left(\frac{\partial T}{\partial t}+\nabla T\cdot\mathbf{v}\right)=k_l\nabla^2 T, \tag{2}$$

where T is the temperature, $\mathbf{v}$ is the velocity of the fluid caused by the density change, k_l the thermal conductivity and c_l the specific heat. Since the geometry is spherical and the temperature applied on the surface $R_b(t)$ is constant, we may assume spherical symmetry. The velocity may be written as $\mathbf{v}=(\mathbf{v}(\mathbf{r}),\mathbf{0},\mathbf{0})$ and the heat equation becomes

$$\rho_l c_l\left(\frac{\partial T}{\partial t}+v\frac{\partial T}{\partial r}\right)=k_l\frac{1}{r^2}\frac{\partial}{\partial r}\left(r^2\frac{\partial T}{\partial r}\right)\quad\text{on}\quad R(t)<r<R_b(t). \tag{3}$$

This is the standard heat equation with advection see Alexiades and Solomon (1993), Natale et al. (2010) and Yang et al. (2003) for example.

Under the assumption of incompressible flow, the velocity $\mathbf{v}$ can be determined from the continuity equation $\nabla\cdot\mathbf{v}=\mathbf{0}$. In the present case,

$$\frac{1}{r^2}\frac{\partial}{\partial r}\left(r^2 v\right)=0 \tag{4}$$

leading to

$$v=\frac{c_0}{r^2} \tag{5}$$

where c_0 is a constant of integration. Mass conservation requires

$$\frac{\mathrm{d}}{\mathrm{d}t}\left[\rho_s\frac{4}{3}\pi R^3+\rho_l\frac{4}{3}\pi\left(R_b^3-R^3\right)\right]=0 \tag{6}$$

this provides an equation for the velocity of the outer surface

$$\frac{\mathrm{d}R_b}{\mathrm{d}t}=-\frac{R^2}{R_b^2}\left(\frac{\rho_s}{\rho_l}-1\right)\frac{\mathrm{d}R}{\mathrm{d}t}. \tag{7}$$

Noting that $v(R_b)=\mathrm{d}R_b/\mathrm{d}t$ provides an expression for c_0 in (5) and so the velocity

$$v=-\frac{R^2}{r^2}\left(\frac{\rho_s}{\rho_l}-1\right)\frac{\mathrm{d}R}{\mathrm{d}t}. \tag{8}$$

The temperature in the solid phase, θ, is given by the one-dimensional heat equation

$$\rho_s c_s\frac{\partial\theta}{\partial t}=k_s\frac{1}{r^2}\frac{\partial}{\partial r}\left(r^2\frac{\partial\theta}{\partial r}\right)\quad\text{on}\quad 0<r<R(t). \tag{9}$$

To avoid having to solve a thermal problem before the melting begins, we will take the initial solid temperature to be $\theta(r,0)=T_m(0)$. The appropriate boundary conditions for Eqs. (3) and (9) are

$$T(R_b,t)=T_H,\quad T(R,t)=\theta(R,t)=T_m(t),\quad \left.\frac{\partial\theta}{\partial r}\right|_{r=0}=0, \tag{10}$$

where $T_m(t)$ is given by Eq. (1).

Energy conservation across the surface $R(t)$ gives the Stefan condition

$$\rho_s\left[L_f+(c_l-c_s)(T_m-T_m^*)\right]\frac{\mathrm{d}R}{\mathrm{d}t}+\frac{\rho_s}{2}\left(1-\frac{\rho_s}{\rho_l}\right)^2\left(\frac{\mathrm{d}R}{\mathrm{d}t}\right)^3=k_s\frac{\partial\theta}{\partial r}\bigg|_{r=R}-k_l\frac{\partial T}{\partial r}\bigg|_{r=R}. \quad (11)$$

A detailed derivation of the Cartesian version of this equation, with $\Delta c=0$, is given in Alexiades and Solomon (1993), and we have simply generalised this to the spherical form.

Equation (11) contains a term that generally does not appear in the Stefan condition, namely the one involving R_t^3. This appears due to the kinetic energy which is a result of the density change forcing the fluid to move. Equation (8) shows the fluid velocity to be proportional to R_t, and hence, the kinetic energy is proportional to R_t^2; the rate of change of mass is also proportional to R_t, hence the cubic dependence. In general, this term may appear to be of less importance than the standard first term on the left-hand side, since the first term appears to be of order L_f greater than the cubic term (for fluids typically $L_f\sim 10^5$). However, it is well known that the standard Stefan problem, with a fixed temperature boundary condition, will have $R_t\to-\infty$ as $t\to 0$ and so, the cubic term will dominate for at least a short period. The spherical Stefan problem has also been shown to have $R_t\to-\infty$ as the melting reaches completion Font and Myers (2013) and McCue et al. (2009).

Equation (1), with $\kappa=1/R(t)$, and Eq. (11) provide relations for the two unknowns $T_m(t)$, $R(t)$. The temperature gradients in (11) come from the solution of the liquid and solid heat equations. The radius is subject to the initial condition $R(0)=R_0$, while $T_m(0)$ is determined by setting $R=R_0$ in Eq. (1).

The above governing equations may be nondimensionalised by introducing the variables

$$\hat{T}=\frac{T-T_m^*}{T_H-T_m^*},\quad \hat{\theta}=\frac{\theta-T_m^*}{T_H-T_m^*},\quad \hat{r}=\frac{r}{R_0},\quad \hat{t}=\frac{k_l}{\rho_l c_l R_0^2}t. \quad (12)$$

The nondimensional moving boundaries are $\hat{R}=R/R_0$ and $\hat{R}_b=R_b/R_0$. Dropping the hats, the governing Eqs. (3) and (9) become

$$\frac{\partial T}{\partial t}-(\rho-1)\frac{R^2}{r^2}\frac{\mathrm{d}R}{\mathrm{d}t}\frac{\partial T}{\partial r}=\frac{1}{r^2}\frac{\partial}{\partial r}\left(r^2\frac{\partial T}{\partial r}\right),\quad R<r<R_b \quad (13)$$

$$\frac{\partial\theta}{\partial t}=\frac{k}{\rho}\frac{1}{r^2}\frac{\partial}{\partial r}\left(r^2\frac{\partial\theta}{\partial r}\right),\quad 0<r<R. \quad (14)$$

The Stefan condition is

$$\rho[\beta+(1-c)T_m]\frac{\mathrm{d}R}{\mathrm{d}t}+\gamma\left(\frac{\mathrm{d}R}{\mathrm{d}t}\right)^3=k\frac{\partial\theta}{\partial r}\bigg|_{r=R}-\frac{\partial T}{\partial r}\bigg|_{r=R}, \quad (15)$$

and the boundary conditions (10) are

$$T(R_b,t)=1,\quad T(R,t)=\theta(R,t)=-\frac{\Gamma}{R},\quad \frac{\partial\theta}{\partial r}\bigg|_{r=0}=0,\quad T(r,0)=-\Gamma, \quad (16)$$

and the initial condition for the melt front is $R(0)=1$. The dimensionless parameters are defined by

$$\rho=\frac{\rho_s}{\rho_l},\quad k=\frac{k_s}{k_l},\quad \beta=\frac{L_f}{c_l\Delta T},\quad c=\frac{c_s}{c_l} \quad (17)$$

$$\Gamma=\frac{2\sigma_{sl}T_m^*}{R_0\rho_s L_f\Delta T},\quad \gamma=\frac{\alpha_l^3\rho_s}{2R_0^2k_l\Delta T}(\rho-1)^2 \quad (18)$$

where $\Delta T=T_H-T_m^*$ and $\alpha_l=k_l/\rho_l c_l$ is the liquid thermal diffusivity. Note that R_b and R are related by

$$R_b^3=\rho-(\rho-1)R^3 \quad (19)$$

which is obtained by integrating Eq. (7) and applying the condition $R=R_b=1$ at $t=0$.

The problem parameters indicate the importance of the various terms. The density variation is represented by ρ, which also appears in γ. Setting $\rho=1$ removes the advection term from the heat equation and the kinetic energy term from the Stefan condition. The importance of kinetic energy is indicated by γ. As well as depending on $\rho,\gamma\propto 1/R_0^2$, that is the importance of the kinetic energy term increases quadratically as the particle size decreases. In Alexiades and Solomon (1993), it is stated that, in general, the cubic term in the Stefan condition is expected to be negligible compared to the linear term. In the present study, we will show that the kinetic energy term is dominant for particles below 100 nm radius. Further, due to the singularity in R_t at the beginning and end of the melt process, the cubic term is important even for much larger particles.

The vast majority of studies of phase change neglect the density difference between phases, and this is achieved by setting $\rho=1$ (and hence $\gamma=0$). In this limit, the advection term disappears from (13) and the kinetic energy term disappears from Eq. (15), to provide the common form of Stefan problem. For a given material, we may also look at the limit $\gamma\to 0$ by choosing a large particle, $R_0\to\infty$ or a large temperature difference $\Delta T\to\infty$. In this situation, the results do not converge to the results from the Stefan problem with $\rho=1$, since firstly the advection term remains in the liquid heat equation and also γ multiplies R_t, so even though $\gamma\to 0$ the limit γR_t may not tend to zero when $R_t\to\infty$ and kinetic energy still has some small effect.

The ratio of specific heats is denoted $c=c_s/c_l$. In Table 1, we see that $c\approx 0.79$ for gold. A common assumption, at least in the mathematical community, is to

set $c = 1$, which then permits the use of the classical Gibbs–Thomson equation (1) instead of the extended nonlinear form given in Font and Myers (2013). The effect of this approximation on nanoparticle melting has been investigated previously in Font and Myers (2013) and McCue et al. (2009), and in particular, it was shown that for large particles, with $R_0 = 100$ nm, setting $c = 1$ made a negligible difference to melt times, whereas for smaller particles, $R_0 = 10$ nm, a difference of the order 10 % was observed. Since our present focus is on the effect of density change, we will set $c = 1$ from now on, since this permits the use of the simpler version of the Gibbs–Thomson relation and considerably simplifies the analysis.

The ratio of conductivities is denoted $k = k_s/k_l$. This is also often set to unity, but leaving it as its correct value does not affect the solution process. However, it does play an important role when reducing the two-phase model to one-phase (i.e. neglecting the solid temperature) as is carried out in Font and Myers (2013) and Wu et al. (2009). The fact that $k_s > k_l$ is key to the energy conserving model of Myers et al. (2012).

The parameter Γ indicates the effect of melting point depression. If $\Gamma = 0$ then the melt temperature is fixed. In general $\Gamma \propto 1/R_0$ so as the radius decreases Γ increases and melting point depression is more significant.

The Stefan number is denoted by β, for a specific material this varies due to the temperature scale of the process. For a small temperature variation, the Stefan number is large and the melting process is slow. For a large temperature variation, the melt process is fast (although slow and fast are rather relative on the nanoscale). Note, particularly within the engineering community, the Stefan number may be referred to as the inverse of our value, i.e. $\beta = c_l \Delta T/L_f$. With nanoparticles, any small increase above the melt temperature will be sufficient to completely melt the particle (once melting starts melting point depression begins and the process speeds up). Consequently, it makes sense to work in the large β regime, which then allows us to use a perturbation solution method. This will be detailed in the following section, and we will then compare the approximate solution with a full numerical solution which is described in Sect. 4.

3 Perturbation solution

Analytical solutions allow us to understand the important factors within a physical process in a way that numerical solutions cannot. For this reason, we now seek an approximate analytical solution, based on a large Stefan number.

The mathematical description of the problem is given by Eqs. (13)–(15) with boundary conditions (16). Equation (1) relates the melt temperature to the radius $R(t)$. To make analytical progress, we make use of a standard perturbation technique. As in Font and Myers (2013), we consider β to be large for our system (for gold heated 10 K above the bulk melt temperature $\beta \approx 40$) and define a new timescale $t = \beta\tau$. This permits us to assume expansions for the temperatures $\theta = \theta_0 + \theta_1/\beta + \mathcal{O}(1/\beta^2)$ and $T = T_0 + T_1/\beta + \mathcal{O}(1/\beta^2)$. Then, Eqs. (13) and (14) can be expressed as a sequence of simpler problems. For example, the leading order problem (where all terms with a factor $1/\beta^n$, where $n \geq 1$, are neglected) is represented by the steady-state equations

$$0 = \frac{1}{r^2}\frac{\partial}{\partial r}\left(r^2\frac{\partial T_0}{\partial r}\right), \quad 0 = \frac{1}{r^2}\frac{\partial}{\partial r}\left(r^2\frac{\partial \theta_0}{\partial r}\right) \tag{20}$$

with boundary conditions $T_0(R_b, \tau) = 1$, $T_0(R, \tau) = \theta_0(R, \tau) = -\Gamma/R$, and $\theta_{0r}(0, \tau) = 0$. The solution to this system is

$$\theta_0 = -\frac{\Gamma}{R}, \qquad T_0 = -\frac{\Gamma}{R} + \frac{R_b}{R}\frac{(r-R)}{r}\left(\frac{R+\Gamma}{R_b - R}\right). \tag{21}$$

The first-order correction, which includes terms with a factor $1/\beta$, is described by

$$\frac{\partial T_0}{\partial \tau} - (\rho - 1)\frac{R^2}{r^2}\frac{\mathrm{d}R}{\mathrm{d}\tau}\frac{\partial T_0}{\partial r} = \frac{1}{r^2}\frac{\partial}{\partial r}\left(r^2\frac{\partial T_1}{\partial r}\right) \tag{22}$$

$$\frac{\partial \theta_0}{\partial \tau} = \frac{k}{\rho}\frac{1}{r^2}\frac{\partial}{\partial r}\left(r^2\frac{\partial \theta_1}{\partial r}\right) \tag{23}$$

with boundary conditions $T_1(R_b, \tau) = T_1(R, \tau) = \theta_1(R, \tau) = \theta_{1r}(0, \tau) = 0$. The appropriate solutions are

$$T_1 = \frac{(\Gamma + R_b)(R_b - r)(r - R)}{6(R_b - R)^2 r}\left\{\frac{3(\rho - 1)R(\Gamma + R)(R_b - R)}{(\Gamma + R_b)r}\right. \tag{24}$$

$$\left. + \frac{(\rho - 1)R(\Gamma + R)[3 - R(R_b + r + R)]}{R_b^2(\Gamma + R_b)} - r + 2R_b - R\right\}R_\tau, \tag{25}$$

$$\theta_1 = -\frac{\rho}{6k}\frac{\Gamma}{R^2}(R^2 - r^2)R_\tau. \tag{26}$$

Now, substituting $\theta \approx \theta_0 + \theta_1/\beta$ and $T \approx T_0 + T_1/\beta$ into the Stefan condition (15) with the new time scale, we obtain the following equation

$$\frac{\gamma}{\beta^3}\left(\frac{\mathrm{d}R}{\mathrm{d}\tau}\right)^3 + \left\{\rho - \frac{\rho\Gamma}{\beta 3R} + \frac{(R+\Gamma)}{\beta 6R}\left[\frac{(\rho - 1)(3R_b - R^2R_b - 2R^3)}{(R_b - R)}\right.\right.$$
$$\left.\left. + \frac{2(\Gamma + R_b)}{(\Gamma + R)}\right]\right\}\frac{\mathrm{d}R}{\mathrm{d}\tau} + \frac{R_b}{R^2}\frac{(R+\Gamma)}{(R_b - R)} = 0 \tag{27}$$

which is subject to the initial condition $R(0) = 1$. Note, since R_b can be expressed in terms of R via Eq. (19), this is a single ordinary differential equation for the unknown

position $R(t)$. It is possible to also expand R and R_b; however, this makes the calculation more complex and so we do not follow this route. So, the perturbation method has reduced the original problem, specified by two partial differential equations, a first-order ordinary differential equation and an algebraic equation, to a single cubic first-order ordinary differential equation. To solve this equation, we may set $z = \mathrm{d}R/\mathrm{d}\tau$ so that it can be expressed as a cubic polynomial of the form $z^3 + k_1 z + k_2 = 0$. In all cases that we tested, this equation had only one real root, $z_1 < 0$, we then integrated $\mathrm{d}R/\mathrm{d}\tau = z_1$ numerically.

For comparison, in the results section we will show solutions with no density jump between phases. This solution may be found by setting $\rho = 1$ in (27). This also determines $\gamma = 0$ and $R_b = 1$. In this case, Eq. (27) reduces to

$$\left(1 + \frac{1}{3\beta R}\right)\frac{\mathrm{d}R}{\mathrm{d}\tau} + \frac{\Gamma + R}{R^2(1-R)} = 0, \quad R(0) = 1 \tag{28}$$

with solution

$$-\beta(1-R^3) + a(1-R^2) - b(1-R) + b\Gamma \ln\left(\frac{\Gamma+1}{\Gamma+R}\right) = 3\beta\tau \tag{29}$$

where $a = [3\beta(\Gamma+1) - 1]/2$ and $b = (\Gamma+1)(3\beta\Gamma - 1)$. In Sect. 5, we will compare the solutions of (27) with (29) for different parameter values and see how the melting times are affected by neglecting the density jump between phases.

A classical difficulty with the numerical solution of Stefan problems occurs because at $t = 0$ one of the phases may not exist, and thus, the initial conditions are problematic, see Mitchell and Vynnycky (2009) (this issue occurs for any value of β). For this reason, it is often beneficial to carry out a small time analysis of the system to determine the initial behaviour. To achieve this, we rescale time as $t = \delta\hat{\tau}$, where $\delta \ll 1$. It is also useful to rescale the space variable r as $\eta = (r-R)/(R_b - R)$ on $R < r < R_b$ and as $\xi = r/R$ on $0 < r < R$. This transforms (15) into

$$(R_b - R)\left[\rho\beta\left(\frac{\mathrm{d}R}{\mathrm{d}(\delta\hat{\tau})}\right) + \gamma\left(\frac{\mathrm{d}R}{\mathrm{d}(\delta\hat{\tau})}\right)^3\right] = k\frac{(R_b - R)}{R}\frac{\partial\theta}{\partial\xi}\bigg|_{\xi=1} - \frac{\partial T}{\partial\eta}\bigg|_{\eta=0}. \tag{30}$$

The initial condition, $R(0) = 1$, indicates that for small times, R should take the form

$$R = 1 - \lambda(\delta\hat{\tau})^p, \tag{31}$$

where p, λ are constant. Equation (19) indicates $(R_b - R) \approx \lambda(\delta\hat{\tau})^p$ and Eq. (30) may now be written as

$$-\lambda(\delta\hat{\tau})^p\left[\rho\beta\lambda p(\delta\hat{\tau})^{p-1} + \gamma(\lambda p)^3(\delta\hat{\tau})^{3p-3}\right] = k\lambda(\delta\hat{\tau})^p\frac{\partial\theta}{\partial\xi}\bigg|_{\xi=1} - \frac{\partial T}{\partial\eta}\bigg|_{\eta=0}. \tag{32}$$

The difficulty now lies in choosing the appropriate value of p. From a physical standpoint, we know that the melting is driven by the temperature gradient in the liquid, T_η. This causes the motion R_t and so one, or both of the terms on the left-hand side must balance the T_η term. Since $\delta \ll 1$ this requires one of the powers $2p - 1$ or $4p - 3$ to be zero (and hence, the δ term is unity). In other words $p = 1/2$ or $p = 3/4$. In the case of no density jump, $\gamma = 0$, and then, there is only one possibility, namely $p = 1/2$. However, when $\gamma \neq 0$ the second term is largest, and so we must choose $p = 3/4$. This means that for small times, the radius decreases as

$$R \approx \begin{cases} 1 - \lambda_1 t^{3/4} & \text{if} \gamma \neq 0 \\ 1 - \lambda_2 t^{1/2} & \text{if} \gamma = 0. \end{cases} \tag{33}$$

The corresponding velocities take the form $R_t \sim t^{-1/4}, t^{-1/2}$ for $\gamma \neq 0$ and $\gamma = 0$ respectively. Both solution forms indicate an infinite velocity as $t \to 0$, but the decrease in radius is faster with no density change (which then results in faster melting). Note, we have not yet determined the constants λ_1, λ_2, and this will be dealt with in the following section.

4 Numerical solution method

The full problem requires the solution of the heat equations in the liquid and solid over an a priori unknown domain, which is determined by the Stefan condition. The solution may be achieved via a finite difference scheme after applying a number of transformations.

Firstly, the temperature variables are changed to $v = r\theta$ and $u = rT$. This is a standard transformation which converts the spherical heat equation into the planar equivalent. The variables $\eta = (r-R)/(R_b - R)$ and $\xi = r/R$ which were defined earlier to obtain the perturbation solution may be used to immobilise the boundaries of u and v, respectively. This leads to the following governing equations

$$\frac{\partial v}{\partial t} = \frac{R_t}{R}\xi\frac{\partial v}{\partial\xi} + k\frac{1}{R^2}\frac{\partial^2 v}{\partial\xi^2} \quad \text{on} \quad 0 < \xi < 1 \tag{34}$$

and

$$(R_b - R)^2\frac{\partial u}{\partial t} = \frac{\partial^2 u}{\partial\eta^2} - \frac{(\rho-1)(R_b-R)^2R^2}{[R + \eta(R_b - R)]^3}R_t u + (R_b - R) \times \left\{\left[1 + \frac{(\rho-1)R^2}{[R+\eta(R_b-R)]^2} - \eta\right]R_t + \eta R_{bt}\right\}\frac{\partial u}{\partial\eta} \tag{35}$$

on $0<\eta<1$. These two equations are subject to the boundary conditions $v(0,t)=0, v(1,t)=u(0,t)=-\Gamma$ and $u(R_b,t)=R_b$. The initial conditions will be discussed below. The Stefan condition may now be written as

$$\rho\beta R^2\frac{\mathrm{d}R}{\mathrm{d}t}+\gamma R^2\left(\frac{\mathrm{d}R}{\mathrm{d}t}\right)^3=k\left.\frac{\partial v}{\partial\xi}\right|_{\xi=1}-\frac{R}{(R_b-R)}\left.\frac{\partial u}{\partial\eta}\right|_{\eta=0}+(k-1)\Gamma \tag{36}$$

where $R(0)=1$.

A semi-implicit scheme may now be employed on the system, discretising implicitly for u,v and explicitly for R,R_t in (34)–(35). The discrete forms of the partial derivatives are

$$\frac{\partial v}{\partial t}=\frac{v_i^{n+1}-v_i^n}{\Delta t},\qquad \frac{\partial v}{\partial\xi}=\frac{v_{i+1}^{n+1}-v_{i-1}^{n+1}}{2\Delta\xi},$$
$$\frac{\partial^2 v}{\partial\xi^2}=\frac{v_{i+1}^{n+1}-2v_i^{n+1}+v_{i-1}^{n+1}}{\Delta\xi^2} \tag{37}$$

where $i=1,\ldots,I$ and $n=1,\ldots,N$, and analogously for u. Using these derivative definitions, Eqs. (34)–(35) can be expressed as a matrix system which are solved at each time step n. The position of the melt front is obtained from (36) using the time derivative

$$\frac{\mathrm{d}R}{\mathrm{d}t}=\frac{R^{n+1}-R^n}{\Delta t} \tag{38}$$

and a three point backward difference for the partial derivatives.

As mentioned earlier, the initial condition can be problematic. There are two reasons for this: firstly, the liquid phase does not even exist at $t=0$; secondly, there is a discontinuity between the imposed boundary condition $u(R_b,t)=R_b$ and the initial condition $u(r,0)=-\Gamma$ which results in an infinite velocity at $t=0$. So, in order to specify a numerical scheme that does not immediately blow up conditions must be determined for some small time $t>0$, where a liquid phase exists and the velocity may be large, but not infinite. This may be achieved utilising the limiting cases discussed in the previous section. Substituting (33) into (35) and (36) and allowing $t\to 0$ leads to the following boundary value problem for temperature in the liquid when $\gamma\neq 0$

$$\frac{\mathrm{d}^2u}{\mathrm{d}\eta^2}=0,\quad u(0)=-\Gamma,\quad u(1)=1,\quad \left(\frac{3}{4}\right)^3\lambda_1^4\rho=\left.\frac{\mathrm{d}u}{\mathrm{d}\eta}\right|_{\eta=0}. \tag{39}$$

This has the solution

$$u=(\Gamma+1)\eta-\Gamma,\quad \lambda_1=\left(\frac{4}{3}\right)^{3/4}\left(\frac{\Gamma+1}{\rho}\right)^{1/4}. \tag{40}$$

Note, the above expression determines λ_1 for Eq. (33).

In the case $\gamma=0$ we obtain

$$\frac{d^2u}{d\eta^2}-\frac{\lambda_2^2}{2}(1-\eta)\frac{\mathrm{d}u}{\mathrm{d}\eta}=0,\quad u(0)=-\Gamma,\quad u(1)=1,$$
$$\beta\frac{\lambda_2^2}{2}=\left.\frac{\mathrm{d}u}{\mathrm{d}\eta}\right|_{\eta=0}. \tag{41}$$

Although more complex than the previous case, this is a standard thermal problem with solution

$$u=1-(1+\Gamma)\frac{\mathrm{erf}\,(\lambda_2(1-\eta)/2)}{\mathrm{erf}\,(\lambda_2/2)} \tag{42}$$

where λ_2 satisfies the transcendental equation

$$\frac{1}{2}\sqrt{\pi}\,\beta\,\lambda_2\,\mathrm{e}^{\lambda_2^2/4}\mathrm{erf}(\lambda_2/2)=1+\Gamma. \tag{43}$$

The numerical scheme may now be started at some small time $t>0$ using Eqs. (40) and (42)–(43) to provide the appropriate temperatures and so avoiding the possible singular behaviour at $t=0$.

5 Results and discussion

In this section, we present a set of results for the melting of a spherical nanoparticle. We use data appropriate for gold (as shown in Table 1) since this is a very common material for nanoparticles. The density change between solid and liquid gold is within the range of many materials, so it provides typical results.

In Fig. 2, we plot the evolution of the solid–liquid interface, $R(t)$, for a nanoparticle with initial dimensional radius 100 nm and $\beta=100$ (which corresponds to relatively slow melting). Two pairs of curves are shown, one for the case $\rho=1$, and the other using the correct value for gold, $\rho\approx 1.116$. The solid lines represent the solution of the equations derived from the perturbation analysis, i.e. the solution for $\rho=1$ given by (29), the other for $\rho=1.116$ given by (27), and the dashed line is the numerical solution. In both cases, the perturbation solution is very close to the numerical solution, indicating a full numerical analysis is not necessary. It is quite clear that the two sets of solutions lead to very different melt times. When $\rho=1$ the melt process lasts until $t\approx 4$, with the correct change in density the process lasts until $t\approx 4.7$, an approximately 15 % increase. Note, we define the melt time as being the time when our calculation stops (in this case $R\approx 0.004$, below this value the Gibbs–Thomson relation (1) predicts a negative melt temperature). As stated in the introduction, the continuum model only holds down to around $R=2$ nm. In fact, we expect complete melting (or dissipation of the particle) to occur somewhere between 2 and 0 nm but given that as $R\to 0$ the melt velocity $R_t\to$

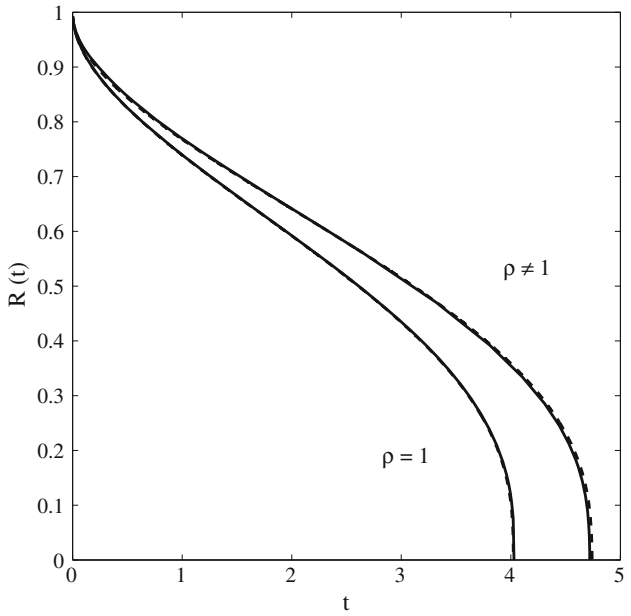

Fig. 2 Evolution of the nondimensional melting front $R(t)$ for the two cases of study $\rho = 1.116$ and $\rho = 1$, for $\beta = 100$ and $R_0 = 100$ nm. *Solid line* represents perturbation solution, *dashed lines* the numerical solution

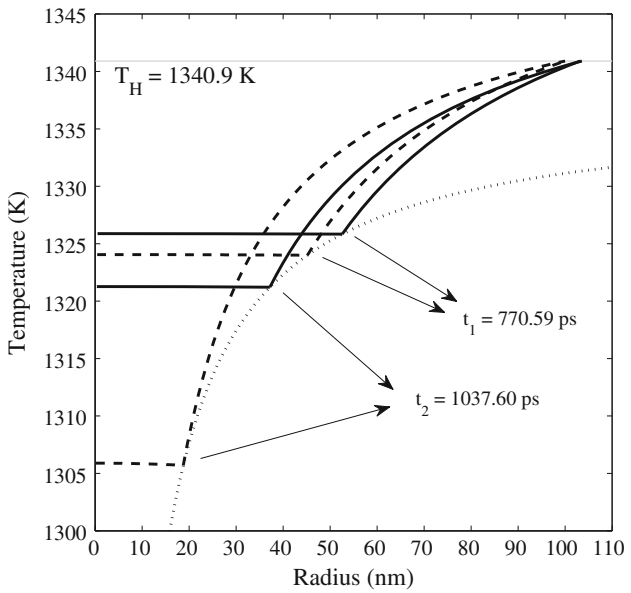

Fig. 3 Dimensional temperature profiles for curves of Fig. 2. The *solid line* represents temperature for $\rho = 1.116$, the *dashed line* $\rho = 1$ and *dotted line* shows the melt temperature variation

$-\infty$ an estimate based on our final value will be very accurate. (If we actually stop the calculation at $R = 2/100$ we find a melt time 0.05 % below that predicted by stopping at $R = 0.004$.) Both sets of curves show a melt velocity $R_t \to -\infty$ in the final stages of melting. We associate this with the sudden melting of nanoparticles as

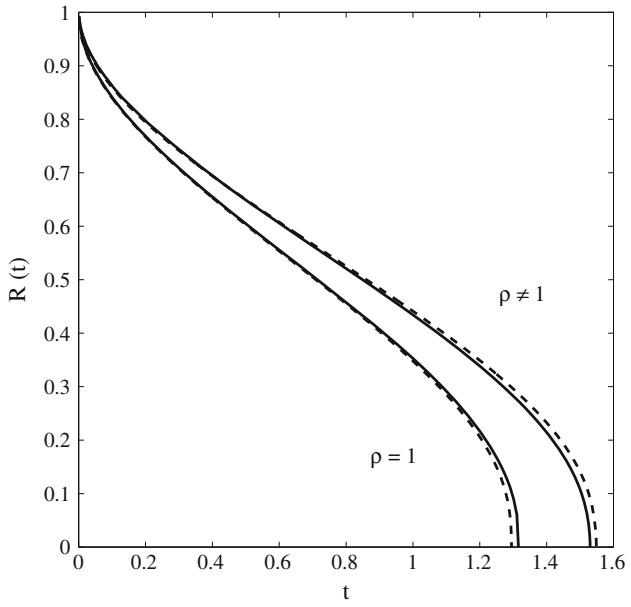

Fig. 4 Evolution of the nondimensional melting front $R(t)$ for $\rho = 1$ and $\rho = 1.116$, for $\beta = 10$ and $R_0 = 100$ nm

$R \to 0$, observed experimentally in Kofman et al. (1999) and already discussed and analysed in previous theoretical studies Back et al. (2014), Font and Myers (2013) and McCue et al. (2009).

In Fig. 3, we present the dimensional temperature profiles corresponding to the curves in Fig. 2. We choose the dimensional form to better show the temperature variation and typical times. The curves all come from the numerical solution: the solid line represents the case where $\rho \approx 1.116$ while the dashed line is $\rho = 1$. The dotted line shows the evolution of the melt temperature as the radius decreases. Temperature profiles are shown for two times, $t = 770.59, 1037.6$ ps. The dashed lines range between 0 and 100 nm, while the solid lines have a moving right-hand boundary ($R_b = R_b(t)$) and so end at $R_b > R_0$.

In Fig. 4, we present two sets of results for the same initial radius, but now $\beta = 10$. Since $\beta \propto 1/\Delta T$ we expect faster melting than in the previous example and this is obviously the case. Since the perturbation expansion is based on $1/\beta$ it is no surprise that the dashed line is slightly further from the solid line than in Fig. 2, and however, the accuracy is still good. Again there is a rapid decrease in radius during the final moments, and so, we expect the final melting time to be very accurate, whether measured at $R = 2/100$ or closer to $R = 0$.

Figures 5, 6 and 7 show results for a particle with initial radius $R_0 = 10$ nm. All features are qualitatively similar to those of the 100 nm particle figures, with an obvious reduction in melt times. In the case of Fig. 5, where $\beta = 100$, ending the calculation close to $R = 0$ or at

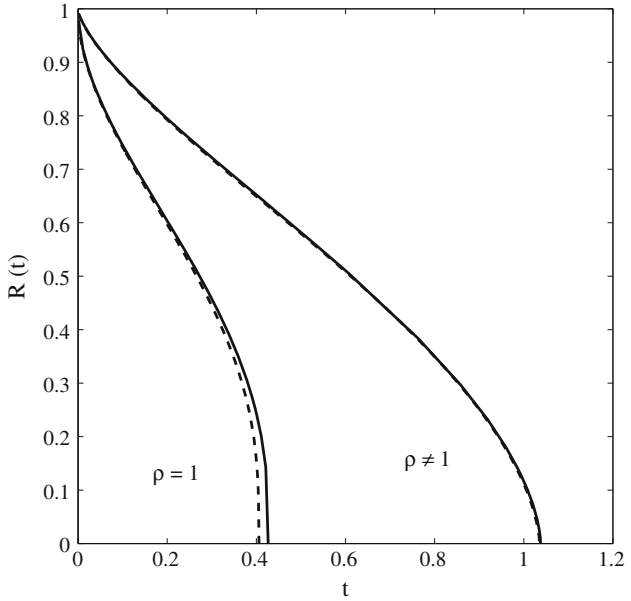

Fig. 5 Evolution of the nondimensional melting front $R(t)$ for $\rho = 1.116$ and $\rho = 1$, for $\beta = 100$ and $R_0 = 10$ nm. *Solid line* represents perturbation solution, *dashed lines* the numerical solution

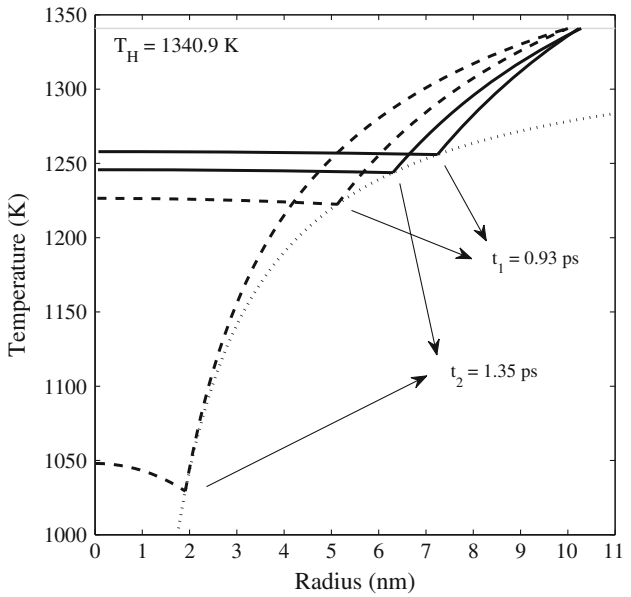

Fig. 6 Dimensional temperature profiles for curves of Fig. 5. The *solid line* represents temperature for $\rho = 1.116$, the *dashed line* $\rho = 1$ and *dotted line* shows the melt temperature variation

$R = 2/10$ results in a 7 % difference in melt times. Choosing $\rho = 1$ rather than the true value will give a more than 55 % decrease in melt time. In Fig. 7, where $\beta = 10$, the decrease is >60 %. Figure 6 shows the temperature profiles corresponding to Fig. 5. An interesting feature is that it is clear the temperature in the solid is greater than the melt temperature and so the solid acts to increase the

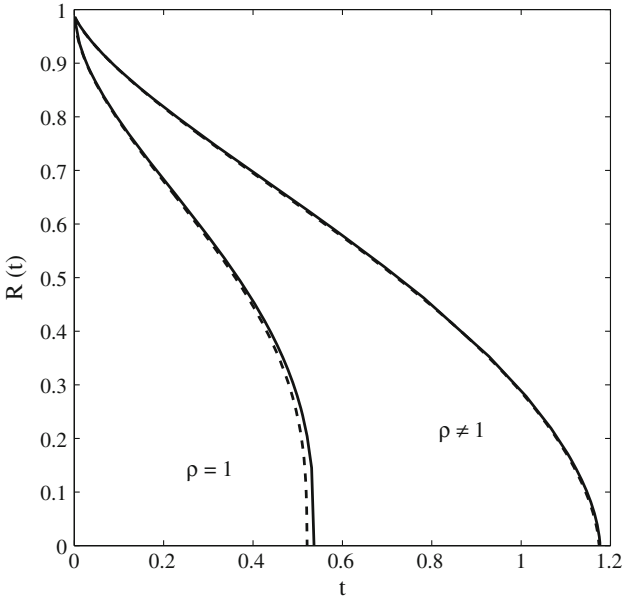

Fig. 7 Evolution of the nondimensional melting front $R(t)$ for $\rho = 1.116$ and $\rho = 1$, for $\beta = 10$ and $R_0 = 10$ nm. *Solid line* represents perturbation solution, *dashed lines* the numerical solution

melt rate (this is also the case in Fig. 3, but less obvious). In standard situations, where T_m is constant, the solid acts to slow down melting.

In Tables 2 and 3, we present dimensional melting times for particle radii 10, 50, 100 nm and $\beta = 5, 10, 100$ for $\rho = 1$ and $\rho = 1.116$, respectively. The dimensional times are obtained by multiplying the nondimensional melting time by the timescale $\rho_l c_l R_0^2/k_l$. By comparing the two tables, we see that for a particle with $R_0 = 10$ nm, the computed melting times for the case $\rho = 1$ are between 56 % (for $\beta = 100$) and 65 % (for $\beta = 5$) faster than for the ones corresponding to $\rho = 1.116$. In the second column ($R_0 = 50$ nm), the melting times for the case $\rho = 1$ are between the 16 and 23 % faster than those for $\rho = 1.116$. Finally, the third column ($R_0 = 100$ nm) shows differences between the two cases of 15 and 16 %. Results for larger particles show that the difference settles at approximately 15 %. This difference in melt times carries through to the macro-scale, indicating the importance of incorporating density variation within more standard Stefan problems.

The physical mechanism behind the slower melting when $\rho = 1.116$ is easily explained by considering the energy in the system. Melting occurs due to heat being input at the boundary R_b. When $\rho = 1$ this energy goes to heating up the material and driving the phase change. However, when $\rho = 1.116$ the fluid must move due to the expansion (or contraction depending on the material) caused by the phase change. This provides another energy sink, namely kinetic energy, which then results in less

Table 2 Melting times for the case $\rho = 1$. Results for gold

	Melting times (s)		
	$R_0 = 10$ nm	$R_0 = 50$ nm	$R_0 = 100$ nm
$\beta = 100$ ($T_H \approx 1341$ K)	1.38×10^{-12}	1.55×10^{-10}	1.07×10^{-9}
$\beta = 10$ ($T_H \approx 1376$ K)	1.08×10^{-12}	0.69×10^{-10}	0.34×10^{-9}
$\beta = 5$ ($T_H \approx 1415$ K)	0.89×10^{-12}	0.45×10^{-10}	0.21×10^{-9}

Table 3 Melting times for the case $\rho = 1.116$. Results for gold

	Melting times (s)		
	$R_0 = 10$ nm	$R_0 = 50$ nm	$R_0 = 100$ nm
$\beta = 100$ ($T_H \approx 1341$ K)	3.12×10^{-12}	1.84×10^{-10}	1.26×10^{-9}
$\beta = 10$ ($T_H \approx 1376$ K)	2.75×10^{-12}	0.85×10^{-10}	0.41×10^{-9}
$\beta = 5$ ($T_H \approx 1415$ K)	2.49×10^{-12}	0.58×10^{-10}	0.25×10^{-9}

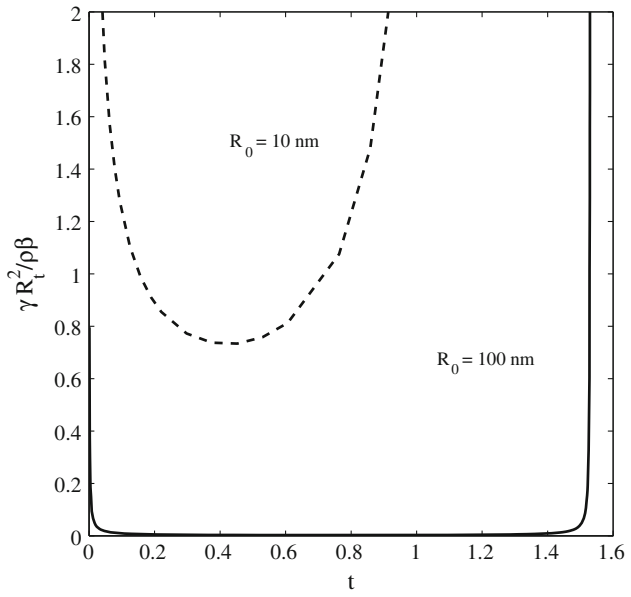

Fig. 8 Relative importance of the term γR_t^3 against $\rho\beta R_t$ for $\beta = 10$, for nanoparticles with radius $R_0 = 100$ nm (*solid line*) and $R_0 = 10$ nm (*dashed line*)

energy available to melt the material. Mathematically, we can see from Eq. (33) that when $\rho = 1$ the initial melt rate $R_t \propto t^{-1/2}$ is much greater than when $\rho = 1.116, R_t \propto t^{-1/4}$.

In Fig. 8, we demonstrate the relative strength of the two terms constituting the left-hand side of Eq. (15), which represent latent heat release and kinetic energy, for the cases where $R_0 = 10, 100$ nm and $\beta = 10$. The dashed line shows the result for $R_0 = 10$ nm. Since its value is close to or greater than unity throughout the melt process, this signifies the cubic term is generally dominant. When $R_0 = 100$ nm the cubic term is negligible for most of the process, but the peaks at the beginning and end mean that it still plays an important role there. Decreasing γ further will push the position of the peaks towards the initial and final times, but will never remove them. Consequently, kinetic energy will always play some role in the energy balance provided $\gamma \neq 0$.

With no experimental results which exactly describe our theoretical models, we must rely on similar studies to provide estimates and at least quantitative agreement. For instance, in Plech et al. (2004), the melting of gold nanoparticles is studied experimentally by time-resolved X-ray scattering when heated up by a laser beam. They find that the time to complete melting is <100 ps for nanoparticles with $R_0 = 50$ nm. In Ruan et al. (2007), the melting of 2 and 20 nm gold nanoparticles is studied, finding melting times on the picosecond scale. Our results show indeed the right order of magnitude, and however, we are not aware of the existence of any experimental studies that could further validate the accuracy of our results.

6 Conclusions

The main aim of this paper was to determine whether the standard modelling assumption that the density remains constant throughout the phase change is valid in the context of nanoparticle melting. Our results clearly show that as the particle radius decreases, the effect of the density change becomes increasingly important. We presented results for the melting of gold and found that melt times for a particle with initial radius 10 nm were more than doubled when the density ratio was changed from $\rho = 1$ to $\rho \approx 1.116$. This increase in melt time may be attributed to the fact that with $\rho = 1$ the liquid phase remains stationary so all energy input into the system is converted to heat or to drive the phase change. If $\rho = 1.116$ then the liquid is forced to move which requires kinetic energy and means less energy is available for the phase change.

We therefore conclude that any mathematical model of nanoparticle melting should incorporate density variation. In fact, our results show an even stronger conclusion, namely that in general, the density variation should be included in phase change models regardless of size. In the case studied in the present paper, the difference in melt times (neglecting or including density variation) tended to a limit of approximately 15 % as the particle size increased.

Acknowledgments The research of TGM was supported by a Marie Curie International Reintegration Grant *Industrial applications of moving boundary problems* Grant No. FP7-256417 and Ministerio de Ciencia e Innovación Grant MTM2011-23789. FF acknowledges the support of a Centre de Recerca Matemàtica PhD grant. SLM acknowledges the support of the Mathematics Applications Consortium for Science and Industry (MACSI, www.macsi.ul.ie) funded by

the Science Foundation Ireland Mathematics Initiative Grant 12/IA/1683. The authors acknowledge Gloria Garcia for her contribution in the art work of the manuscript.

References

Alexiades V, Solomon AD (1993) Mathematical modelling of freezing and melting processes. Hemisphere Publishing Corporation, Washington

Back JM, McCue SW, Hsieh MH-N, Moroney TJ (2014) The effect of surface tension and kinetic undercooling on a radially-symmetric melting problem. Appl Math Comput 229:41–52

Buffat P, Borel JP (1976) Size effect on the melting temperature of gold particles. Phys Rev A 13(6):2287–2297

Charach C, Rubinstein I (1992) Pressure–temperature effects in planar Stefan problems with density change. J Appl Phys 71:1128

Davis SH (2001) Theory of solidification. Cambridge University Press, Cambridge

Font F, Myers TG (2013) Spherically symmetric nanoparticle melting with a variable phase change temperature. J Nanopart Res 15(12):1–13

Font F, Mitchell SL, Myers TG (2013) One-dimensional solidification of supercooled melts. Int J Heat Mass Transf 62:411–421

Guisbiers G, Kazan M, Van Overschelde O, Wautelet M, Pereira S (2008) Mechanical and thermal properties of metallic and semiconductive nanostructures. J Phys Chem C 112:4097–4103

Kofman R, Cheyssac P, Lereah Y, Stella A (1999) Melting of clusters approaching 0D. Eur Phys J D 9:441–444

Lai SL, Guo JY, Petrova V, Ramanath G, Allen LH (1996) Size-dependent melting properties of small tin particles: nanocalorimetric measurements. Phys Rev Lett 77(1):99–102

McCue SW, Wu B, Hill JM (2009) Micro/nanoparticle melting with spherical symmetry and surface tension. IMA J Appl Math 74:439–457

Mitchell SL, Vynnycky M (2009) Finite-difference methods with increased accuracy and correct initialization for one-dimensional Stefan problems. Appl Math Comput 215(4):1609–1621

Myers TG, Low J (2011) An approximate mathematical model for solidification of a flowing liquid in a microchannel. Microfluid Nanofluid 11:417–428

Myers TG, Low J (2013) Modelling the solidification of a power-law fluid flowing through a narrow pipe. Int J Thermal Sci 70:127–131

Myers TG, Mitchell SL, Font F (2012) Energy conservation in the one-phase supercooled Stefan problem. Int Commun Heat Mass Transf 39(10):1522–1525

Nanda KK (2009) Size dependent melting of nanoparticles. Pramana J Phys 72(4):617–628

Natale MF, Santillan Marcus EA, Tarzia DA (2010) Explicit solutions for one-dimensional two-phase free boundary problems with either shrinkage or expansion. Nonlinear Anal Real World Appl 11:1946–1952

Ockendon J, Lacey A, Movchan A, Howison S (1999) Applied partial differential equations. Oxford University Press, Oxford

Plech A, Kotaidis V, Grésillon S, Dahmen C, Von Plessen G (2004) Laser-induced heating and melting of gold nanoparticles studied by time-resolved X-ray scattering. Phys Rev B 70(19):195423

Ruan C, Murooka Y, Raman RK, Murdick RA (2007) Dynamics of size-selected gold nanoparticles studied by ultrafast electron nanocrystallography. Nano Lett 7(5):1290–1296

Travis KP, Todd BD, Evans DJ (1997) Departure from Navier–Stokes hydrodynamics in confined liquids. Phys Rev E 55(4):4288–4295

Wu B, McCue SW, Tillman P, Hill JM (2009) Single phase limit for melting nanoparticles. Appl Math Model 33(5):2349–2367

Wu B, Tillman P, McCue SW, Hill JM (2009) Nanoparticle melting as a Stefan moving boundary problem. J Nanosci Nanotechnol 9(2):885–888

Yang Z, Sen M, Paolucci S (2003) Solidification of a finite slab with convective cooling and shrinkage. Appl Math Model 27:733–762